The TR-808 Cymbal: a Physically-Informed, Circuit-Bendable, Digital Model

Kurt James Werner, Jonathan S. Abel, Julius O. Smith
Center for Computer Research in Music and Acoustics (CCRMA)
Stanford University, Stanford, California
[kwerner|abel|jos]@ccrma.stanford.edu

ABSTRACT

We present an analysis of the cymbal voice circuit from a classic analog drum machine, the Roland TR-808 Rhythm Composer. A digital model based on this analysis (implemented in Cycling 74's Gen~) retains the salient features of the original. Developing physical models of the device's many sub-circuits allows for accurate emulation of circuit-bent modifications (including component substitution, changes to the device's architecture, and voltage starve)—complicated behavior that is impossible to capture through black-box modeling or structured sampling. This analysis will support circuit-based musicological inquiry into the history of analog drum machines and the design of further mods.

1. INTRODUCTION

Despite significant work that has been done on cloning and emulating the TR-808, there is an almost complete lack of published analyses on the circuit. [1] We have begun to fill this void with [3], which develops a physically-informed, circuit-bendable, digital model of the TR-808's bass drum voice circuit. In the following paper, we will use related techniques (well-represented in virtual analog literature) to analyze the 808's cymbal voice circuit.

The goals of this research are to partition the 808's cymbal circuit into functional blocks, create a physically-informed analysis of each block, model each block in software, and evaluate the results. Throughout, we will pay special attention to developing an analysis in terms of the electrical values of circuit elements.

It is particularly important to analyze the 808 in this way, because of the extant misinformation surrounding the device. [2] The 808's rich mythology has been well-covered in music journalism, but this has distracted from focused study of the individual voice circuits. The 808's cymbal voice circuit represents a significant leap forward in the design of analog drum machine voices—it is a complex, efficient circuit that reasonably approximates a real cymbal sound.

The 808 cymbal has only a few user-controllable parameters: decay, tone, and level. To access the latent potential of the circuit, drum machine modders add additional tuning and architecture-level controls, even going so far as to allow external audio to be routed through the circuit [6]. This tradition parallels the development of circuit-bending and other music hardware hacking, and could potentially be lost in the process of digitally emulating an 808.

By adopting a physically-informed approach, and favoring an analysis that elucidates the design intent, this work supports informed mods of the circuit. A more complicated analysis could obscure the logic of the device's construction, with minimal gains in accuracy. Framing the analysis in terms of component values simplifies the simulation of mods based on component substitution. [3] Partitioning the circuit into blocks allows for the simulation of mods based on changes to the circuit's architecture. [4]

We give an overview of the circuit in §2 and an analysis of each part of the circuit and their interconnections in §§3–11. This is followed by a discussion of modeling techniques in §12 and results in §13.

2. OVERVIEW

Fig. 1 shows a schematic diagram of the TR-808 cymbal circuit. This annotated schematic labels important nodes and currents, and shows how the circuit is broken down into blocks: Schmitt trigger oscillators (see §3), band pass filters (see §4), trigger logic (see §5), an attack smoother (see §6), envelope generators (see §7), "swing-type voltage-controlled amplifiers" (VCAs, see §8), high pass filters (see §9), a tone control stage (see §10), and an output buffer and level control (see §11). Fig. 2 shows a block diagram of the digital model of the cymbal circuit. Both figures

[1] previous work includes [2], which offers a qualitative discussion of [1] in the context of imitating classic synthesized cymbal voices with modular synthesizers

[2] For instance: the user manual for the Novation Drum Station (an early rack-mount TR-808/TR-909 emulator) says the cymbal sound is generated by "multiple noise sources," which is patently false. Some improbable stories about the machine's design turn out to be true. Don Lewis, an early pioneer of drum machine modification, worked on the design of the 808 and even developed techniques that influenced its voice design [4]. He relates a story from his visit to Roland's Tokyo offices in the late 70s, where he worked with chief engineer Tadao Kikumoto. "That day he had a bread board of an 808 and was showing me what was going on inside–he sort of bumped up against the breadboard and spilled some tea in there and all of a sudden he turned it on and got this *pssh* sound–it took them months to figure out how to reproduce it, but that ended up being the crash cymbal in the 808. There was nothing else like it. Nobody could touch it." [5]

[3] for instance: adding tuning controls to the oscillators, band pass filters, and high pass filters; additional controls to the static envelope generators; or extending the tone controls.

[4] for instance: allowing each of the 6 rectangular wave oscillators or the bands to be individually muted, bypassing filters, or injecting external audio.

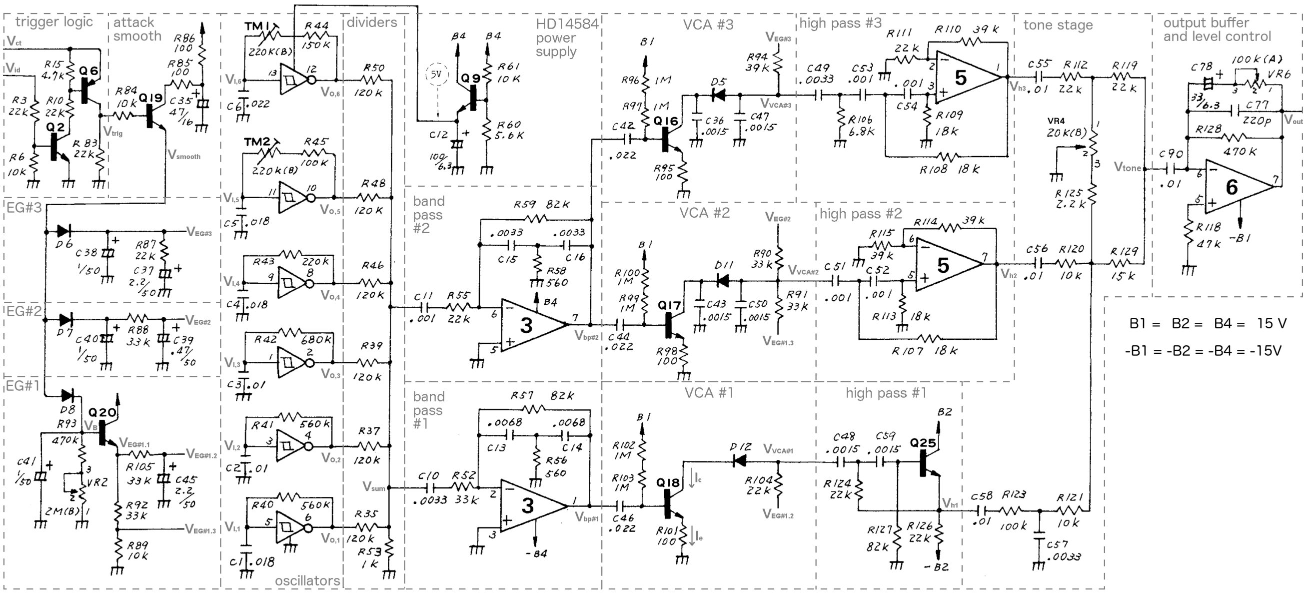

Figure 1. TR-808 cymbal schematic (adapted from [1]).

should be consulted alongside the analysis of each block in the following sections.

To produce a cymbal note, the μPD650C$-$085 CPU applies a common trigger and (logic high) instrument data to the trigger logic. The resulting 1-ms long pulse is delivered to the envelope generators via an attack smoother. The output of this smoother drives four envelope signals, which are applied to three swing-type VCAs, where they control the amplitude of three bands of filtered rectangular wave clusters. Two different active band pass filters sum and filter the output of six Schmitt trigger inverter oscillators, producing these clusters. The output of each of the three swing-type VCAs is applied to a corresponding Sallen-Key high pass filter. From there, each band is applied to a tone control stage and a level control, which sums the three bands back together and buffers the output.

3. SCHMITT TRIGGER OSCILLATORS

The TR-808's Cowbell, Cymbal, Open Hihat, and Closed Hihat voice circuits all work by filtering and enveloping rectangular waves. In fact, they all share a common bank of six of these oscillators, ingeniously implemented with a single HD14584 hex Schmitt trigger inverter chip. In each of these astable multivibrators, the Schmitt trigger inverter acts as the bistable element, and a passive network of a single resistor and capacitor provides an RC time constant that tunes the oscillator to a particular frequency. [5]

Oscillators #1–4 are hardwired to a particular frequency. The last two, which form the basis of the Cowbell voice circuit, are tunable via trimpots that are only accessible by opening up the TR-808's internals. Although this was intended for factory tuning, early drum machine hackers were quick to pull these controls out to the front panel. [6] This primarily had the effect of a producing a tunable cowbell voice. However, they also form an important part of the cymbal sound as well. [7]

The inverter has only low and high output states (V_{OL} and V_{OH}), and transitions between them are subject to hysteresis. When an input voltage V_I rises above a positive-going threshold voltage V_{T+}, the output swings to V_{OL}. When V_I falls below a negative-going threshold voltage V_{T-}, the output swings to V_{OH}. [8]

Since the positive-going and negative-going threshold voltages for a Schmitt trigger input are different, the circuit will oscillate back and forth as the capacitor is alternatively charged and discharged. Considering the continuous-time cases of a charging and discharging capacitor separately yields the capacitor charge and discharge times:

$$t_{\text{charge}} = RC \cdot \ln\left(\frac{V_{OH} - V_{T-}}{V_{OH} - V_{T+}}\right) \tag{1}$$

$$t_{\text{discharge}} = RC \cdot \ln\left(\frac{V_{OL} - V_{T+}}{V_{OL} - V_{T-}}\right). \tag{2}$$

These times sum to the total period of oscillation $T = t_{\text{charge}} + t_{\text{discharge}}$. Since the oscillator switches between output states V_{OL} and V_{OH}, its amplitude is trivially equal to their difference. The duty cycle is, by definition, the proportion of time that the oscillator spends in its high state. Now, the salient features (frequency $f = {}^1\!/_T$, amplitude $A = V_{OH} - V_{OL}$, and duty cycle $D = {}^{t_{\text{charge}}}\!/_T$) are avail-

[5] This technique was well-known to hardware hackers as early as the 1960s, and forms an important building block of so-called "Lunetta Synths"—CMOS-based devices inspired by the designs of Stanley Lunetta.

[6] Nowadays, this technique is well-documented among hackers and creators of 808 clones and emulators. See: [7], Tactile Sounds' TS-808, Analogue Solutions' Concussor, Acidlab's Miami, &c.

[7] Robin Whittle points to component tolerance (and, by extension, variations in tuning for oscillators #5–6) as the source of the unique character of individual 808 cymbals [6].

[8] The switching characteristics (output rise and fall time, propagation delay time [8]) of the HD14584 are all faster than 250 ns, and the transitions are smooth. Keeping in mind the bandwidth of human hearing (roughly, 20–20,000 hertz, corresponding to a minimum period of 50 μs), this transition is treated as instantaneous. We forego alias-suppressed methods for rectangular wave simulation (for instance: [9]), since the aliased components will be sufficiently filtered out or perceptually masked downstream.

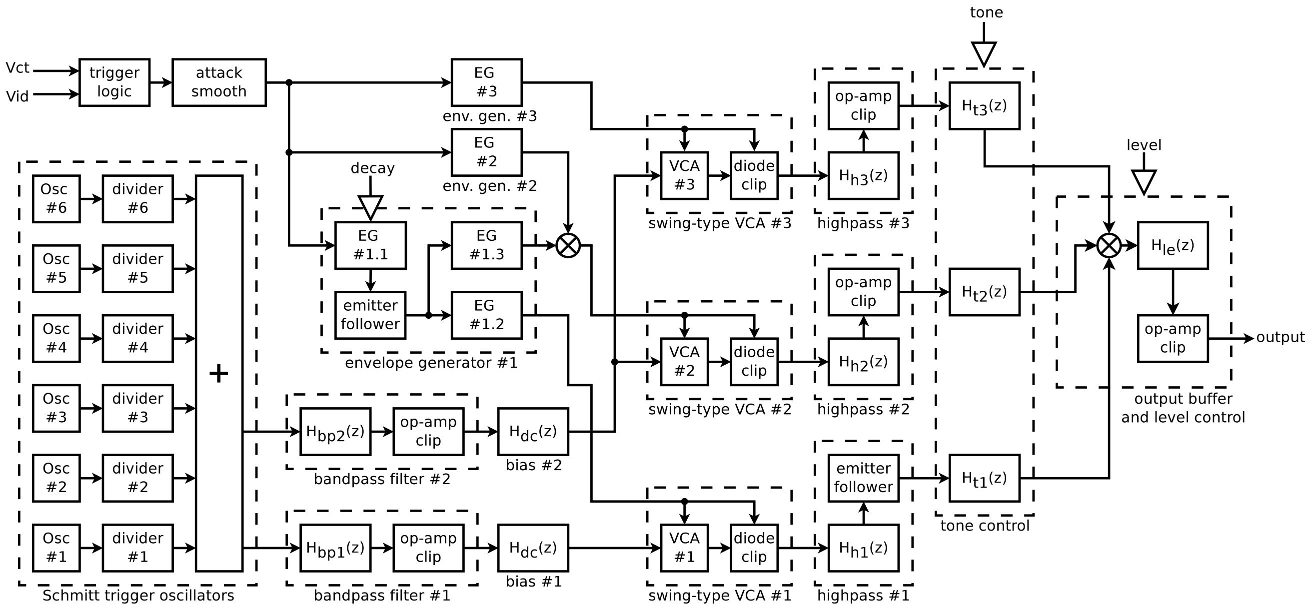

Figure 2. TR-808 cymbal emulation block diagram.

able in terms of passive component values and the device properties of the Schmitt trigger inverter.

Plugging in Equations (1)–(2) to the definition of duty cycle, the time constant RC drops out—the duty cycle depends only on the inverter's device properties V_{T-}, V_{T+}, V_{OL}, and V_{OH}:

$$D = \ln\left(\frac{V_{OH}-V_{T-}}{V_{OH}-V_{T+}}\right) \Big/ \ln\left(\frac{(V_{OH}-V_{T-})(V_{OL}-V_{T+})}{(V_{OH}-V_{T+})(V_{OL}-V_{T-})}\right) . \quad (3)$$

The six oscillators have nominal frequencies (or ranges) of 205.3, 369.6, 304.4, 522.7, 359.4–1149.9, and 254.3–627.2 Hz. Oscillators #5–6 have internal trimpots (TM_2 and TM_1) in series with their resistor, for factory tuning to specific frequencies (800 and 540 Hz, respectively). [9]

By design, the HD14584 is powered with 5 volts, yielding a duty cycle of $D = 47.98\%$ and an amplitude of $A = 5$ volts for each oscillator. [10]

All six oscillators are summed via voltage dividers in a passive mixing network. The output of this network is applied to the input of the band pass filters. Respecting superposition (grounding the other oscillator outputs), an example calculation of this attenuation (for oscillator #1) is:

$$\frac{V_{\text{sum}}}{V_{O,1}} = \frac{R_{53}}{R_{53} + (R_{37} \parallel R_{39} \parallel R_{46} \parallel R_{48} \parallel R_{50})} . \quad (4)$$

Fig. 3 shows a comparison between the sum of all six oscillators (the signal applied to each band pass filter) and tabulated data from a SPICE [11] simulation of the circuit. [12]

[9] Early manufacturing runs (prior to serial #000300) used different values for the resistors and capacitors in oscillators 5 and 6 [1].

[10] using the "typical" values from the device's datasheet [8]

[11] **S**imulation **P**rogram with **I**ntegrated **C**ircuit **E**mphasis, a widely-used family of general purpose analog electronic circuit simulators.

[12] No attempt was made to align the phase of the model to the tabulated SPICE data. Fig. 3 just shows, qualitatively, that the model and the reference SPICE simulation have similar features.

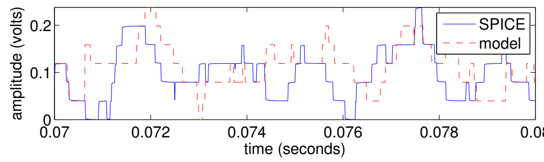

Figure 3. Sum of all oscillators (V_{sum}).

4. BAND PASS FILTERS

The two active band pass filters [13] each filter the combination of the six rectangular waves. What follows is a representative analysis and simulation of band pass filter #1. Identical methods were used for #2.

Assuming ideal op-amp behavior, nodal analysis of band pass filter #1 yields a transfer function of the form:

$$H_{bp1}(s) = \frac{V_{bp\#1}}{V_{\text{sum}}} = \frac{\beta_2 s^2 + \beta_1 s}{\alpha_3 s^3 + \alpha_2 s^2 + \alpha_1 s + \alpha_0} , \quad (5)$$

with coefficients:

$$\begin{aligned}
\beta_2 &= -R_{56}R_{57}(C_{13}+C_{14})C_{10} \\
\beta_1 &= -R_{57}C_{10} \\
\alpha_3 &= R_{56}R_{57}R_{52}C_{13}C_{14}C_{10} \\
\alpha_2 &= R_{56}R_{57}C_{13}C_{14} + R_{56}R_{52}(C_{13}+C_{14})C_{10} \\
\alpha_1 &= R_{56}C_{13} + R_{56}C_{14} + R_{52}C_{10} \\
\alpha_0 &= 1 .
\end{aligned}$$

Fig. 4 shows the magnitude response of each band pass filter. Band pass filter #1 has a center frequency around 3440 Hz and band pass filter #2 has a center frequency around 7100 Hz. These band pass filters strongly accentuate the upper overtones of the square waves, while de-emphasizing their fundamental frequencies.

[13] whose topologies are closely related to the so-called "bridged-T network", a bridged-T Zobel network in the negative-feedback path of an op-amp, that is used in each of the 808's voice circuits [3]

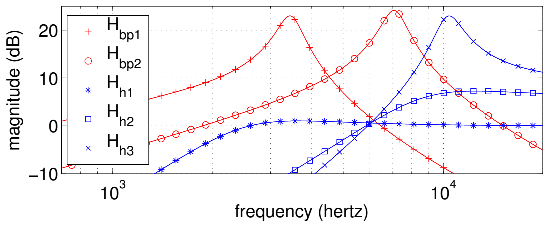

Figure 4. Magnitude responses of band pass and high pass filters.

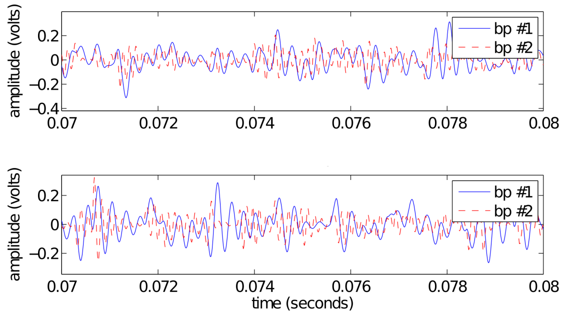

Figure 5. Band pass response in time domain, physical model (top) and SPICE (bottom).

Fig. 5 shows typical behavior in the time domain. Each time one of the six rectangular wave oscillators flips state, the edge kicks some more AC energy into each band pass filter.

5. TRIGGER LOGIC

The 808's sequencer controls the timing and amplitude of each voice circuit via the CPU. The CPU produces a timing signal and accent signal, which are combined into a common trigger signal V_{ct}, whose ON voltage is set by VR_3, a user-controllable global accent level. In general, instrument timing data (unique to each voice) sequenced by the CPU is "ANDed" with V_{ct} to activate individual voice circuits.

In the case of the cymbal, the circuit comprised of Q_2, Q_6, R_3, R_6, R_{10}, R_{15}, and R_{83} "ANDs" the instrument data V_{id} with a buffered version of V_{ct} (with its range narrowed to 7–14 V, depending on VR_3 [1]). When V_{id} is present (logic high), a 1-ms long pulse is passed to the collector of Q_6.

The effect of the varying accent level is complex, and depends heavily on nonlinear downstream subcircuits: the attack smoother, envelope generators, and the swing-type VCAs.

6. ATTACK SMOOTHER

The circuit comprised of Q_{19}, R_{84}–R_{86}, and C_{35} "smooths" the attack of V_{trig}, the pulse that the trigger logic produces. Although the physics of this sub-circuit are difficult to work out in closed form, a one pole filter of the following form approximates the behavior of this circuit:

$$H_{as}(s) = \frac{V_{smooth}}{V_{\mathrm{trig}} - V_{BE}} = \frac{1}{1+\tau s}\,, \tag{6}$$

where V_{BE} is the voltage drop from the base of Q_{19} to its emitter, and τ is an RC time constant. The values of these constants are found by least-squares minimization to be:

$$V_{BE} = 0.7258\,, \qquad \tau = 1.0244 \cdot 10^{-4}\,.$$

Fig. 6 shows good agreement between this simplified model and tabulated data from SPICE.

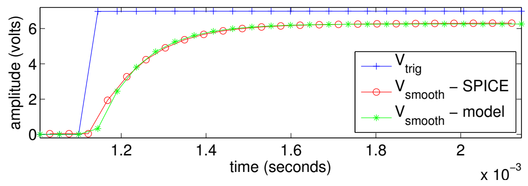

Figure 6. Attack smoother output, no accent, time domain.

7. ENVELOPE GENERATORS

The attack smoother applies a smoothed trigger V_{smooth} to three envelope generators via D_6–D_8. These envelopes serve as amplitude control for each swing-type VCA. What follows is a representative analysis and simulation of envelope generator #1. Identical methods were used for #2–3.

In envelope generator #1, an emitter follower buffers the first stage (EG #1.1). The output of the emitter follower drives two more stages (EG #1.2 and EG #1.3).

The first stage EG #1.1 is comprised of D_6, R_{93}, VR_2, and C_{41}. A simplified diode model [14] is leveraged to separate the attack and release phases, allowing simulation by numerical solution of a switched first-order ordinary differential equation (ODE).

During the attack phase (while $V_B < V_{\mathrm{smooth}} - V_{\mathrm{on}}$, and D_8 acts as a short), an equation that approximates V_B is:

$$V_B = V_{\mathrm{in}} - V_{\mathrm{on}}\,. \tag{8}$$

During the release phase (while $V_B > V_{\mathrm{smooth}}$, and D_6 acts as an open circuit), nodal analysis yields:

$$\frac{\mathrm{d}V_B}{\mathrm{d}t} = -\frac{V_B}{\mathrm{VR}_2 k R_{93} C_{41}}\,, \tag{9}$$

where $\mathrm{VR}_2 k$ is the resistance of the decay control with maximum resistance VR_2 and knob position $k \in [0.0, 1.0]$. At higher decay settings, the RC time constant of decay increases, and the decay for this band is longer.

V_{on} is estimated in the least-squares sense by a fit to tabulated data from a SPICE simulation during the attack portion on the envelope. This yields $V_{\mathrm{on}} = 0.5899$.

[14] One that assumes the diode spends little time around the corner of its I–V characteristic and can be treated as a switch:

$$R_{diode} = \begin{cases} \infty & \text{if} \quad V_{diode} < V_{on} \\ 0 & \text{if} \quad V_{diode} \geq V_{on} \end{cases} \tag{7}$$

.

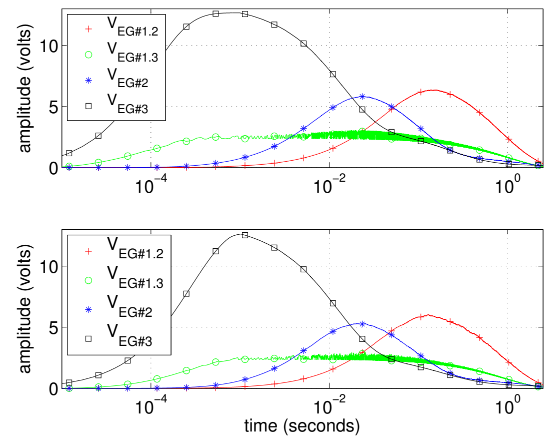

Figure 7. Log time envelope signals, physical model (top) and SPICE simulation (bottom).

An emitter follower Q_{20} produces $V_{\mathrm{EG\#1.1}}$, a buffered version of V_B. Its output is taken at Q_{20}'s emitter, with a voltage gain of ≈ 1 and a negative offset V_{BE}. V_{BE} is estimated just like V_{on}, which yields $V_{BE} = 0.6195$.

The output of this emitter follower is applied to two passive RC networks, EG #1.2 and EG #1.3. Nodal analysis yields a continuous-time transfer function and a memoryless relationship:

$$H_{\mathrm{EG\#1.2}} = \frac{V_{\mathrm{E3\#1.2}}}{V_B} = \frac{R_{104}}{sR_{104}R_{105}C_{45} + R_{104} + R_{105}} \quad (10)$$

$$H_{\mathrm{EG\#1.3}} = \frac{V_{\mathrm{E3\#1.3}}}{V_B} = \frac{R_{89}R_{91}}{R_{89}R_{91} + R_{89}R_{92} + R_{91}R_{92}} . \quad (11)$$

$H_{\mathrm{EG\#1.2}}$ is a high shelf filter, and $H_{\mathrm{EG\#1.3}}$ is a simple passive voltage divider. Each part of the envelope circuit is solved numerically in time by using the explicit Forward Euler method. [15]

Fig. 7 shows good agreement between the time domain behavior of the physical model's envelope generators and a reference SPICE simulation. The traces are plotted in log time to show more detail towards the start of the envelopes.

8. SWING-TYPE VCAS

So-called swing-type VCAs [16] perform nonlinear voltage-controlled amplification. They resemble common-emitter amplifiers, despite their non-standard biasing scheme, extra diode, and the fact the V_{CC} has been replaced by an applied envelope voltage. What follows is a representative analysis and simulation of swing-type VCA #1. Similar methods were used for #2–3. [17]

An analysis and close approximation to the behavior of a swing-type VCA is found by framing it as a modified common-emitter amplifier, working through its biasing details, performing a large-signal DC analysis when the transistor is in forward-active operation, and estimating a memoryless nonlinearity to approximate the behavior of the diode and the transistor's saturation region operation.

8.1 VCA biasing

R_{102}–R_{103} and C_{46} form a DC blocking high pass filter, with an offset V_B (which is estimated like before).

This kind of biasing scheme is inherently unstable to temperature change, and depends strongly on the Bipolar Junction Transistor's (BJT) β parameter, which varies significantly from component to component. For this reason, this sort of biasing is usually discouraged [10]. Here, it leads to clipping—a wild swing of the output between $V_{\mathrm{EG\#1.2}}$ and $V_{\mathrm{lowerEdge}}$, apparent intended behavior.

8.2 Large-Signal DC Analysis

A BJT in forward-active operation is partially described by an equation (an approximation to the Ebers-Moll model) relating the emitter current i_E to the voltage drop from the base to the emitter, V_{BE}:

$$i_E = I_{ES}\left(e^{\frac{V_{BE}}{V_T}} - 1\right) , \quad (12)$$

where I_{ES} is the reverse saturation current of the base–emitter p–n junction [18] and V_T is the thermal voltage. [19]

Since i_B is much smaller than the others, it is reasonable to approximate $i_C = i_E$ via KCL. Now, ignoring output loading, we can get a naïve expression for V_{out} by finding the voltage drop across the collector resistor R_{104}:

$$V_{estimated\#1} = V_{\mathrm{EG\#1.2}} - R_{104}I_{ES}\left(e^{\frac{V_{BE}}{V_T}} - 1\right) . \quad (13)$$

8.3 VCA Nonlinearity

The diode gates the output when $V_{\mathrm{EG\#1.2}}$ is low enough. Without the diode, the output of the VCA would never shut all the way off. The approximation in Equation (13) is fairly accurate for negative values of V_{BE}. However, it takes neither the gating action of the diode nor the fact that the transistor can operate in the saturation region into account. These two behaviors are approximated by estimating the lower edge of the output as a function of $V_{\mathrm{EG\#1.2}}$ and calculating the output voltage $V_{VCA\#1}$ as a nonlinear function of $V_{\mathrm{EG\#1.2}}$, $V_{\mathrm{lowerEdge}}$ and $V_{\mathrm{estimated\#1}}$.

Unsurprisingly (due to the presence of two p–n junctions), $V_{\mathrm{lowerEdge}}$ is well-approximated by the sum of two stretched exponential functions and an offset:

$$V_{\mathrm{lowerEdge}} = \alpha_0 e^{-\beta_0 V_{\mathrm{EG\#1.2}}{}^{\gamma_0}} + \alpha_1 e^{-\beta_1 V_{\mathrm{EG\#1.2}}{}^{\gamma_1}} + \alpha_2 . \quad (14)$$

Curve-fitting [20] yields the coefficients shown in Table 1.

The clipping behavior of the diode and the transistor's behavior in its saturation region are approximated by a nonlinear equation of V_{env}, $V_{\mathrm{lowerEdge}}$ and $V_{\mathrm{estimated\#1}}$:

$$V_{\mathrm{VCA\#1}} = \frac{V_{\mathrm{estimated\#1}} - V_{\mathrm{env}}}{\left(1 + \left|\frac{V_{\mathrm{estimated\#1}} - V_{\mathrm{env}}}{V_{\mathrm{env}} - V_{\mathrm{lowerEdge}}}\right|^{\alpha}\right)^{\frac{1}{\alpha}}} + V_{\mathrm{env}} . \quad (15)$$

[15] $x(n+1) = x(n) + T \cdot f(x(n))$

[16] This odd name is given by [1]. §8.1 should offer a clue to its meaning.

[17] For swing-type VCA #2, there are two envelope sources (EG #1.2 and EG #2). For swing-type VCAs #2–3, there are additional capacitors to ground around the diodes, so analysis is complicated slightly, requiring the use of ODEs.

[18] normally between 10^{-12}–10^{-15} amperes

[19] a function $V_T = {}^{kT}/_{q}$ of temperature, Boltzmann's constant $k \approx 1.3806 \cdot 10^{23}$ joules/kelvin, and the charge of an electron $q \approx 1.6022 \cdot 10^{19}$ coulombs. $V_T \approx 25.85$ mV at room temperature (300 K).

[20] via Matlab's `cftool`

i	α_i	β_i	γ_i
0	-1.396	1.063	1.000
1	0.825	0.837	1.447
2	0.566		

Table 1. coefficients for $V_{\text{lowerEdge}}$ fit

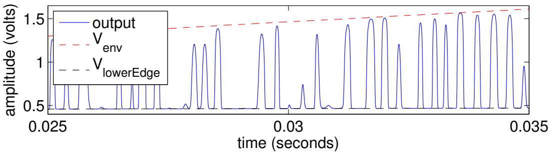

Figure 8. VCA #1 response, time domain detail.

This is a modified version of the clipping equation from [11]. The parameter α controls the "sharpness" of the function's corners. A value of $\alpha = 3.5$ [21] gives a good visual fit to a tabulated SPICE simulation [22] Fig. 8 shows VCA #1's behavior in the time domain.

9. HIGH PASS FILTERS

What follows is a representative analysis and simulation of high pass filter #1. Identical methods were used for #2–3.

High pass filter #1 (H_{h1}) is a 2nd-order high pass Sallen-Key filter [14] with an emitter follower (Q_{25}) as its buffer amplifier element. Assuming the emitter follower acts as a perfect buffer, this yields a continuous-time transfer function [15]:

$$H_{h1}(s) = \frac{V_{\text{h1}}}{V_{\text{VCA\#1}}} = \frac{\beta_2 s^2}{\alpha_2 s^2 + \alpha_1 s + \alpha_0}\,, \tag{16}$$

with coefficients:

$$\begin{aligned}
\beta_2 &= R_{124} R_{127} C_{48} C_{59} \\
\alpha_2 &= R_{124} R_{127} C_{48} C_{59} \\
\alpha_1 &= R_{124} C_{48} + R_{124} C_{59} \\
\alpha_0 &= 1\,.
\end{aligned}$$

High pass filter #2 (H_{h2}) is a 2nd-order, high pass, non-unity-gain Sallen-Key filter with an op-amp as its buffer amplifier element.

High pass filter #3 (H_{h3}) is a 3rd-order high pass Sallen–Key filter with an op-amp as its buffer amplifier element. Using an op-amp in place of an emitter-follower allows for the design of non-unity-gain buffering. This manifests as resonance at the corner frequency (around 10500 Hz) in the magnitude response.

Fig. 4 shows the magnitude responses of the three high pass filters.

10. TONE STAGE

The tone stage is a highly-interconnected passive network of resistors and capacitors, which can be described by three

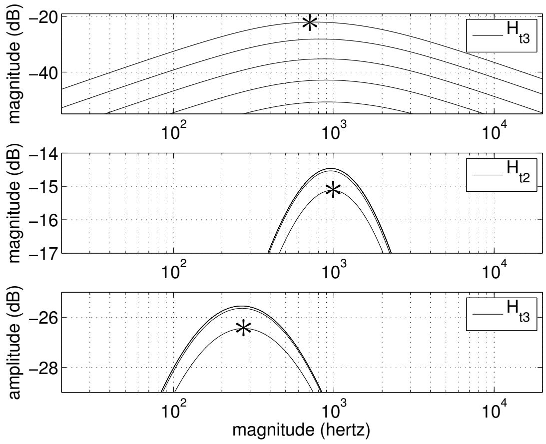

Figure 9. Family of tone stage magnitude responses with tone control $k \in [0.01, 1.0]$. $k = 1.0$ responses are marked with an asterisk ($*$).

transfer functions, $H_{t1} = {}^{V_{\text{tone}}}/_{V_{h1}}$, $H_{t2} = {}^{V_{\text{tone}}}/_{V_{h2}}$, and $H_{t3} = {}^{V_{\text{tone}}}/_{V_{h3}}$. These transfer functions are fifth order, and the expressions for their filter coefficients are far too lengthy to print in this work or to provide much insight by visual inspection. They are reported on this work's companion site. [23]

Fig. 9 shows a family of magnitude responses for each of the three bands. The primary effect of the tone control is to change the amount of attenuation in the third band. However, the center frequencies of all bands and the attenuation of the first and second bands are also somewhat affected. The tone control of the TR-808 cymbal voice shares the property of weakly-separated, non-orthogonal controls with guitar amplifier tone stacks [16].

11. OUTPUT BUFFER AND LEVEL CONTROL

The output buffer sums together the three cymbal bands, through the tone stage, and offers level control. Assuming an ideal op-amp, there will be no current through, and therefore no voltage across, R_{118}. Nodal analysis yields a transfer function of the form:

$$H_{le}(s) = \frac{V_{out}}{V_{t1}} = \frac{\beta_2 s^2 + \beta_1 s}{\alpha_2 s^2 + \alpha_1 s + \alpha_0}\,, \tag{17}$$

with coefficients:

$$\begin{aligned}
\beta_2 &= -R_{128} \mathrm{VR}_6 k C_{90} C_{78} \\
\beta_1 &= -R_{128} C_{90} \\
\alpha_2 &= R_{128} \mathrm{VR}_6 k C_{77} C_{78} \\
\alpha_1 &= (R_{128} + \mathrm{VR}_6)\, C_{78} \\
\alpha_0 &= 1\,.
\end{aligned}$$

where $\mathrm{VR}_6 k$ is the resistance of the level control with maximum resistance VR_6 and knob position $k \in [0.0, 1.0]$. Fig. 10 shows the magnitude response of the transfer functions at various level settings. In addition to attenuation,

[21] This value may be related to the fact that this function approximates hyperbolic trigonometric functions [11], [12], something that would probably arise from the exponential terms in the interaction between two p–n junctions

[22] Due to capacitive loading, and the associated time behavior, it is hard to do a proper least-squares fit (see also: [13]), hence the visual fit.

[23] `https://ccrma.stanford.edu/~kwerner/papers/icmcsmc2014.html`

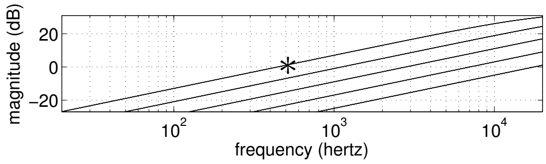

Figure 10. Family of level control magnitude responses with level control $k \in [0.01, 1.0]$. The $k = 1.0$ response is marked with an asterisk $(*)$.

the output level control buffer also acts as a differentiator in the audio band—it has a frequency response with a $^{6\,\mathrm{dB}}/_{\mathrm{octave}}$ rising slope.

12. MODELING

We implemented a digital model with Cycling 74's `Gen~`, a low-level DSP environment in `Max/MSP`. The model contains stock controls for the cymbal decay, tone, and level. Additionally, the model contains bends for tuning and muting individual Schmitt trigger oscillators, tuning or bypassing each band pass and high pass filter, and controlling the release of envelope generators #1 and #3. One bend that has a surprising effect on the sound is replacing R_{53} with a logarithmic potentiometer. Recalling Equation (4), this bend controls the attenuation of each oscillator on its way into the band pass filters and dramatically alters the timbre of the cymbal.

All discrete-time filter coefficients are calculated with the bilinear transform. The bilinear transform is used to map continuous-time transfer functions to discrete time, though it has an inherent frequency warping which adversely affects high frequencies. This frequency warping can be mitigated by oversampling and/or tuning of the bilinear transform's c parameter. By tuning this parameter for each filter, exactly one analog frequency can be precisely mapped to the correct digital frequency (the cutoff or center frequency of a filter gives good results) [17]. [24]

Since many of the filters in the TR-808 cymbal voice circuit have response features that are high in frequency with respect to normal audio sampling rates (i.e. $f_s =$ 44100 Hz), this frequency warping must be addressed. All examples in this work are rendered at $4\times$ oversampling ($f_s = 44100 \times 4$ Hz), so they suffer only negligibly from frequency warping.

There will be some bandwidth expansion in the VCA stage, due to its nonlinearity. Although this creates the potential for aliasing, the cymbal circuit creates tightly-packed, inharmonically-related partials by design. As well, some of the aliasing will be mitigated by the oversampling. Unsurprisingly, the presence of low amplitude aliased frequency components seem to be perceptually insignificant.

Some parts of the model are oversimplified. The VCAs and envelope generators, in particular, are modeled with significant simplifications, and some of their nonlinearities ignored. Non-idealities in high pass filter #1's emitter-follower buffer are ignored. To break the delay-free loops arising from mutual interaction between the VCAs and envelope generators, fictitious unit delays are inserted. Since the envelope signals change very slowly with respect to the sampling rate, the error that is introduced by the unit delays is not very significant. However, in general, inserting fictitious unit delays into systems with feedback can have negative effects on accuracy and stability [18].

13. RESULTS AND CONCLUSIONS

Fig. 11(a) is a spectrogram/waveform pair of a reference cymbal note, produced via SPICE simulation. Fig. 11(b) is the same output from the physical model, which shows good agreement with the SPICE simulation.

Figs. 11(c)–11(f) show some of the bends that are available in the model. These bends can dramatically alter the cymbal's timbre and texture.

Fig. 11(c) shows the effect of disconnecting three of the rectangular wave oscillators, and tuning the remaining three to an open-voiced A major chord. Rather than producing a glut of inharmonically related partials, as in the circuit's stock configuration (or a real, physical cymbal), these harmonically related partials have a comb-filter- or resonator-like effect.

Fig. 11(d) shows the effect of lowering the values of resistors R_{56} and R_{58} by a factor of one half. This raises their center frequencies, affects their Qs, and generally eliminates much of the low-frequency content.

Fig. 11(e) shows the effect of lowering R_{53}. This affects the level of the signal going into the band pass filters, and causes the signal to only sporadically clip in the VCAs—this has an effect on the texture of the output.

Fig. 11(f) shows the effect of a 50% voltage starve. This technique is common in circuit bending and guitar pedal modification [25] but remains unexplored in the context of the TR-808. [26] Lowering the voltage supplied to the HD14584 (by changing voltage divider pair R_{60}–R_{61}) affects the inverter's device properties V_{T^-}, V_{T^+}, V_{OL}, and V_{OH}. [27] This will affect the tuning, amplitude, and duty cycle of each oscillator. Due to the nonlinearity of the VCAs, this will have complex timbral consequences.

Audio examples and other supplementary materials can be found online at this work's companion site. [28]

Acknowledgments

Some preliminary analysis insights were developed with Kevin Tong as part of professor Greg Kovacs's Analog Electronics course. Thanks to Melissa Kagen for help with editing.

[24] `https://ccrma.stanford.edu/~jos/fp/Frequency_Warping.html`

[25] see [19] for an DIY example, and Danelectro's Danelectrode for a commercial example.

[26] although it is hinted at in [7]

[27] A reasonable estimate of these properties as a function of supply voltages in the range 3–15 V is obtained by extrapolation of the electrical characteristics at 5, 10, and 15 volts [8].

[28] `https://ccrma.stanford.edu/~kwerner/papers/icmcsmc2014.html`

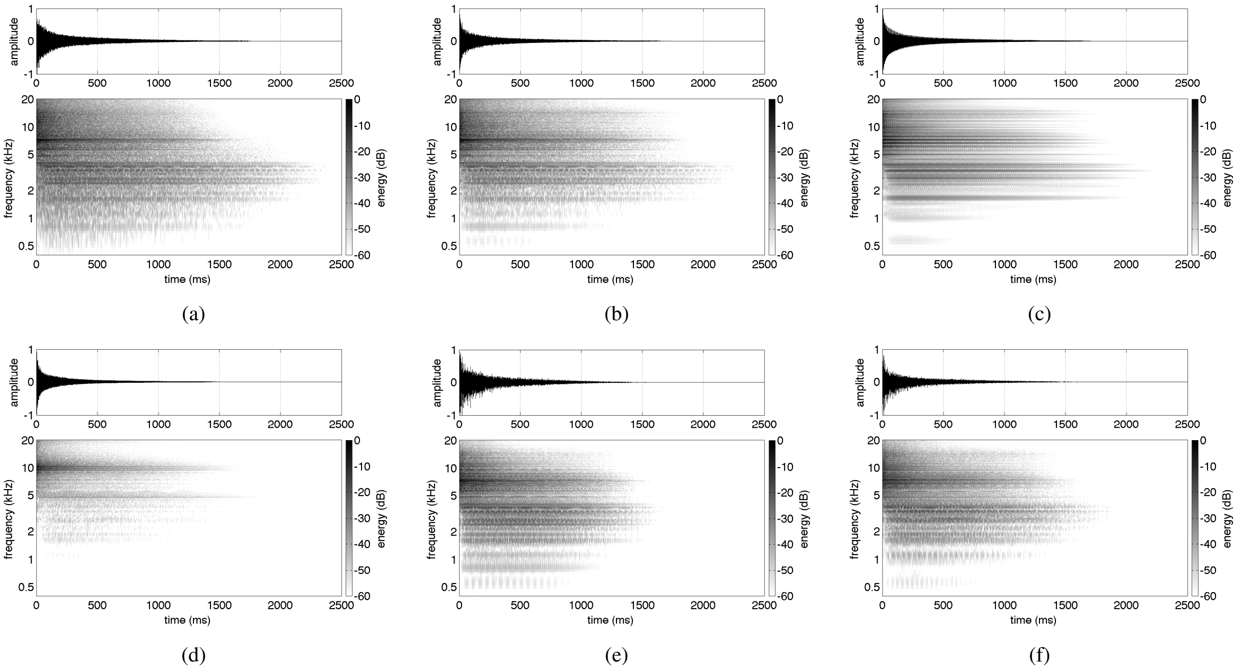

Figure 11. Waveform/spectrogam pairs of cymbal voice circuit simulations: (a) a baseline SPICE simulation for comparison, (b) a baseline emulation with the physically-informed model, (c) muting 3 of the rectangular wave oscillators and tuning the remaining 3 to an A major chord, (d) altering the band pass filter responses by lowering R_{56} and R_{58}, (e) effect of lowering R_{53}, and (f) voltage starve. All are rendered at $4\times$ oversampling, with the decay knob at 25%, tone knob at 50%, and level knob at 50%.

14. REFERENCES

[1] Roland Corporation, "TR-808 Service Notes, 1st ed." June 1981.

[2] G. Reid, "Synth Secrets: Practical Cymbal Synthesis," *Sound on Sound*, July 2002, [Online].

[3] K. J. Werner, J. S. Abel, and J. O. Smith, "A Physically-Informed, Circuit-Bendable, Digital Model of the Roland TR-808 Bass Drum Circuit," in *Proc. Int. Conf. on Digital Audio Effects (DAFx-14)*, Erlangen, Germany, Sept. 1–5, 2014.

[4] D. Lewis, Mar. 15, 2014, private communication.

[5] T. Wolbe, "How the 808 Drum Machine Got Its Cymbal, and Other Tales From Music's Geeky Underbelly," *The Verge*, Jan. 30, 2013, [Online].

[6] R. Whittle, "Modifications for the Roland TR-808," Oct. 7, 2012, [Online]. Available: http://www.firstpr.com.au/rwi/tr-808/.

[7] E. Archer, "TR-808 Cowbell Project," 2009, [Online]. Available: http://ericarcher.net/devices/cowbell/.

[8] Hitachi Semiconductor, "Hex Schmitt Trigger, HD14584B Datasheet," 1999.

[9] T. Stilson and J. O. Smith, "Alias-Free Digital Synthesis of Classic Analog Waveforms," 1996.

[10] P. Horowitz and W. Hill, *The Art of Electronics*, 1st ed. Cambridge University Press, 1980.

[11] D. T. Yeh, J. S. Abel, and J. O. Smith, "Simplified, Physically-Informed Models of Distortion and Overdrive Guitar Effect Pedals," in *Proc. Int. Conf. on Digital Audio Effects*, Bordeaux, France, Sept. 10–15, 2007.

[12] A. Huovilainen, "Non-Linear Digital Implementation of the Moog Ladder Filter," in *Proc. Int. Conf. on Digital Audio Effects (DAFx-7)*, Naples, Italy, Oct. 5–8, 2004.

[13] S. Möller, M. Gromowski, and U. Zölzer, "A Measurement Technique for Highly Nonlinear Transfer Functions," in *Proc. 5th Int. Conf. on Digital Audio Effects (DAFx-02)*, Hamburg, Germany, Sept. 26–28, 2002.

[14] J. Karki, "Analysis of the Sallen-Key Architecture," 2002.

[15] Okawa Electric Design, "Filter Design and Analysis," 2008, [Online]. Available: http://sim.okawa-denshi.jp/en/Fkeisan.htm.

[16] D. T. Yeh and J. O. Smith, "Discretization of the '59 Fender Bassman Tone Stack," in *Proc. Int. Conf. on Digital Audio Effects*, Montreal, Canada, Sept. 18–20, 2006.

[17] J. O. Smith, *Physical Audio Signal Processing*. Available: https://ccrma.stanford.edu/~jos/pasp/, 2010, [Online book].

[18] T. Stilson and J. Smith, "Analyzing the Moog VCF with Considerations for Digital Implementation," in *Proc. Int. Comput. Music Conf. (ICMC-96)*, San Francisco, USA, 1996, pp. 398–401.

[19] D. Beavis, "Building a Dying Battery Simulator: Starve Your Circuit of Power," 2009, [Online]. Available: http://www.beavisaudio.com/projects/DBS/.